



## Article

# Long-Time Persisting Superhydrophilicity on Sapphire Surface via Femtosecond Laser Processing with the Varnish of TiO<sub>2</sub>

Dandan Yan <sup>1,2</sup>, Zhi Yu <sup>1</sup>, Tingting Zou <sup>1</sup>, Yucai Lin <sup>1,2</sup> , Wenchi Kong <sup>1,2</sup> and Jianjun Yang <sup>1,\*</sup>

<sup>1</sup> GPL Photonics Laboratory, State Key Laboratory of Applied Optics, Changchun Institute of Optics, Fine Mechanics and Physics (CIOMP), Chinese Academy of Sciences (CAS), Changchun 130033, China

<sup>2</sup> Center of Materials Science and Optoelectronics Engineering, University of Chinese Academy of Sciences, Beijing 100049, China

\* Correspondence: jjyang@ciomp.ac.cn

**Abstract:** The acquiring of superhydrophilic surfaces attracts the strong interest in self-cleaning, anti-fogging and anti-icing fields based on the unique features. However, the persistent time of superhydrophilic surfaces is still facing a big challenge because of easily adsorbing hydrophobic groups. Here, we propose a strategy to achieve a superhydrophilicity persisting for an unprecedentedly long time on sapphire surfaces, by compounding the femtosecond laser-induced hierarchical structures and the subsequent varnish of TiO<sub>2</sub>. The superhydrophilic effect (with a contact angle of CA = 0°) created by our method can be well prolonged to at least 180 days, even for its storage in air without additional illumination of UV lights. Based on comprehensive investigations, we attribute the underlying mechanisms to the coordination of laser-induced metal ions on the material surface via TiO<sub>2</sub> doping, which not only prevents the adsorption of the nonpolar hydrocarbon groups, but also modulates the photo-response properties of TiO<sub>2</sub>. In addition, further experiments demonstrate the excellent anti-fogging properties of our prepared samples. This investigation provides a new perspective for further enhancing the durability of superhydrophilicity surfaces.



**Citation:** Yan, D.; Yu, Z.; Zou, T.; Lin, Y.; Kong, W.; Yang, J. Long-Time Persisting Superhydrophilicity on Sapphire Surface via Femtosecond Laser Processing with the Varnish of TiO<sub>2</sub>. *Nanomaterials* **2022**, *12*, 3403. <https://doi.org/10.3390/nano12193403>

Academic Editor: Christophe Donnet

Received: 19 August 2022

Accepted: 26 September 2022

Published: 28 September 2022

**Publisher's Note:** MDPI stays neutral with regard to jurisdictional claims in published maps and institutional affiliations.



**Copyright:** © 2022 by the authors. Licensee MDPI, Basel, Switzerland. This article is an open access article distributed under the terms and conditions of the Creative Commons Attribution (CC BY) license (<https://creativecommons.org/licenses/by/4.0/>).

**Keywords:** femtosecond laser; long-time superhydrophilicity; sapphire; TiO<sub>2</sub>

## 1. Introduction

Over decades of years, the superhydrophilicity of material surfaces has attracted great attention in many fields, because of its real significance not only in the fundamental research but also for practical applications such as self-cleaning, anti-fogging, anti-icing, and fluid transport [1–8]. In order to achieve this target, several different methods have been implemented. One is a deposition of molecular films with the pronounced hydrophilic property on the substrate; for example, thiols are commonly used to enhance the surface hydrophilicity of gold, silver, and copper materials [9–13]. The second hydrophilic technique is the hydrophilic treatment by plasma, photons, electrons, ions, and ozone [14–18], which often exhibit disadvantages in both the mechanical strength and the time aging, thus actually impeding their practical applications.

During recent years, the femtosecond laser has proven to be a new powerful tool for high-precision manufacturing, and its unique modifications on both the surface morphology and physicochemical properties demonstrate many potentials in optics, solar-thermal energy technologies, and wettability [19–22]. Usually, however, the lifetime of the obtained superhydrophilic surfaces by laser processing has been found very limited, i.e., for the direct exposing of the laser-processed materials to air, the available surface superhydrophilicity can be maintained only for a few days or even several hours [23–25]. Such a phenomenon has been attributed by many researchers to the adsorption of hydrophobic groups on the structured surfaces [26–29]. In order to settle this problem, Christina et al. tried to increase the surface roughness and surface energy of steel surfaces using the femtosecond laser ablation in a nitrogen environment, resulting in the hydrophilic surface with the contact

angle of  $CA = 24 \pm 3^\circ$  for 101 days [30]. On the other hand, by in situ deposition of  $\text{SiO}_2$  on 316 L stainless steel with the nanosecond laser, Rajab et al reported the superhydrophilic behavior ( $CA < 2^\circ$ ) lasting for six months, which benefits from the high surface energy of silicon and oxygen contents [31]. More recently, Rajan et al. demonstrated the sustainable superhydrophilic property ( $CA = 0^\circ$ ) for about 42 days, when the zeolite films were coated on the surface of aluminum alloys treated by the femtosecond laser [32].

As a matter of fact, the wide bandgap semiconductor  $\text{TiO}_2$  is another category of hydrophilic materials [33], and it was found to display the superhydrophilicity upon irradiation with UV light. By considering the wide potential applications in environmental purification and solar energy conversion [34,35], this discovery has further aroused great research interest. However, such wettability conversion often suffers from certain limitations: the essentially required optical absorption from high-energy photons to create electron-hole pairs because of the large bandgap (3.2 eV) for  $\text{TiO}_2$ ; the short lifetime of superhydrophilicity by the recombination of charge carriers after UV irradiation. For example, the UV-induced superhydrophilic of  $\text{TiO}_2$  films began to fail after storing in darkness for about 10 days, with gradual increasing of the contact angle from  $CA = 0^\circ$  to  $53^\circ$  [36].

To suppress the recombination of photogenerated charge carriers, Watanabe et al. developed a novel  $\text{TiO}_2/\text{WO}_3$  film to improve sensitivity of the superhydrophilic but still with UV illumination, and its superhydrophilic durability was yet unknown [37]. On the other hand, many metal and non-metal ions dopants have been investigated for  $\text{TiO}_2$  to improve the photocatalytic activity [38–41], while few such works were reported on the change of hydrophilicity. In general, seeking a sustainable superhydrophilic effect, especially under no UV light irradiation, is a substantial challenge in current situations.

Based on the above analysis, we here propose a novel strategy of the manipulation on the sapphire surface by femtosecond laser processing associated with the varnish of  $\text{TiO}_2$ , to successfully achieve long-time persisting (at least for 180 days) superhydrophilicity with  $CA = 0^\circ$ . Specifically, the micro/nano-structures were firstly prepared on the sapphire surface by femtosecond laser to show the superhydrophilicity with  $CA = 0^\circ$ . Then, the  $\text{TiO}_2$  precursor solution was spin-coated on its surface and annealed by high temperature to obtain anatase with  $\text{Al}^{3+}$  ions doping, which tends to inhibit the subsequent adsorption of hydrophobic groups. Meanwhile, our sample surface could exhibit a high absorption throughout the UV-Vis range. As a result, an extremely long-lasting superhydrophilicity on the sapphire surfaces could be surprisingly observed. Furthermore, our superhydrophilic surface is experimentally shown to have great anti-fogging potential.

## 2. Materials and Methods

### 2.1. Preparation of Materials

**Substrate material:** A single crystal sapphire wafer (crystal face  $\langle 0001 \rangle$ ) was employed as a sample material, because of its excellent physical, chemical, and optical properties for the wide applications.

**Synthesis of  $\text{TiO}_2$  precursor:** First, HCl solution (35% concentration, CHRON CHEMICALS, Chengdu, China) was diluted to 2 M with deionized water. Then 35  $\mu\text{L}$  2 M HCl was mixed with 2.53 mL anhydrous ethanol ( $\text{CH}_3\text{CH}_2\text{OH}$ ,  $\geq 99.7\%$  concentration, Sinopharm Chemical Reagent, Shanghai, China) in air, which is denoted as solution A. Secondly, 369  $\mu\text{L}$  titanium isopropoxide ( $(\text{CH}_3\text{CH}_2\text{CHO})_4\text{Ti}$ , 95% concentration, Shanghai Aladdin Biochemical Technology, Shanghai, China) was added into 2.53 mL anhydrous ethanol in a glove box, which is denoted as solution B. Finally, solutions A and B were mixed and stirred for 12 h at room temperature.

### 2.2. Femtosecond Laser Processing

A schematic diagram of the experimental setup for the femtosecond laser processing is shown in Figure 1a,b, where a commercial chirped pulse amplification system of Ti: Sapphire laser (Spitfire Ace, Spectra Physics, Milpitas, CA, USA) was employed as a light source at a repetition rate of 1 kHz, with a central wavelength of 800 nm and a pulse time

duration of 40 fs. Each laser pulse delivered from the laser system has the maximum energy of 7 mJ with the linear polarization. In our practical experiments, the laser-pulse energy reduced to a small value of 0.2 mJ by passing through variable attenuators, and then it was focused onto the sapphire surface by a plano-convex optical lens with a focal length of  $f = 100$  mm. The diameter of the focused laser beam was calculated by Zemax software (ANSYS, Canonsburg, PA, USA) to be  $12 \pm 0.6 \mu\text{m}$ , with the corresponding laser energy fluence of  $F = 155 \pm 7.75 \text{ J}/\text{cm}^2$ . The spatial interval between the two adjacent lines was of  $35 \mu\text{m}$  and the scanning speed was varied as  $V = 0.1, 0.3, 0.5 \text{ mm}/\text{s}$ . The direction of the sample scanning was parallel to the laser polarization. Variable micro/nano-structures can be produced on the sapphire surface with different laser-scanning speeds (see Figure S1 from the Supplementary Materials). All the laser-processing experiments were carried out in the atmosphere environment.

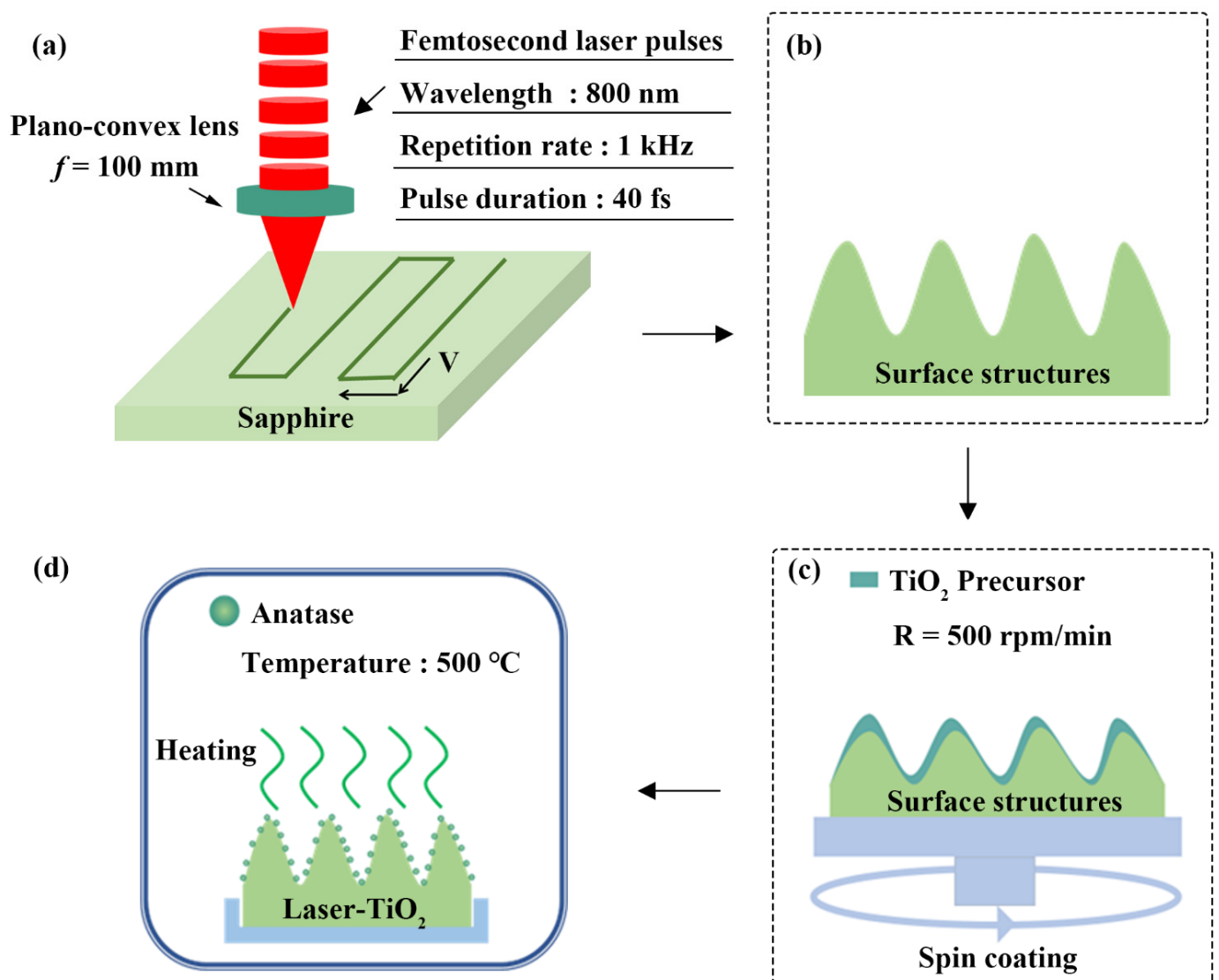


**Figure 1.** (a,b) Schematic diagrams of the femtosecond laser processing on the sapphire surface; (c,d) Preparation procedures for the varnish of  $\text{TiO}_2$  onto the sapphire surface micro/nano-structured by the femtosecond laser.

### 2.3. Varnishing TiO<sub>2</sub> Film on the Sapphire Surface after Laser Processing

The TiO<sub>2</sub> precursor was spin-coated onto the laser-ablated sapphire surface for 30 s at a rotation speed  $R = 500$  rpm/min, then the sample was annealed at 500 °C for 2 h in a muffle furnace, as shown in Figure 1c,d.

### 2.4. Characterizations

The crystalline structure of the materials was characterized by an X-ray diffractometer (XRD, Bruker D8 Advance, Karlsruhe, Germany), with a measurement range of  $2\theta = 20\text{--}90^\circ$ . The surface morphology was analyzed by a field emission scanning electron microscope (SEM, Zeiss, Oberkochen, Germany). Elemental distribution was measured by using the Energy Dispersive Spectrometer (EDS, Zeiss, Oberkochen, Germany). The chemical compositions of the materials were analyzed by X-ray photoelectron spectroscopy (XPS, Thermo Fisher Scientific, Waltham, MA, USA), whose source gun type is Al K Alpha with a stepping energy of 0.05 eV. A video surveillance-based contact angle measuring instrument (Powereach, Shanghai, China) was used to characterize the surface wettability. The optical absorption of the samples was measured with a UV-Vis-NIR spectrophotometer (Agilent, Santa Clara, CA, USA).

## 3. Results and Discussion

### 3.1. Superhydrophilicity Obtained on Sapphire Surface by Laser Processing

At first, we prepared a superhydrophilic surface with  $CA = 0^\circ$  (see video S1 from the Supplementary Materials) on the sapphire material by the laser ablation processing. However, we found an increase in the contact angle with its storage time in air (Figure S2 from the Supplementary Materials), which means that such superhydrophilic property of  $CA = 0^\circ$  is only temporary and cannot be maintained in a long term. According to the previous studies [42,43], the adsorption of nonpolar hydrocarbon groups on the material surface is also responsible for the transition from the superhydrophilic to the superhydrophobic. The observation of this fact in our experiments was shown in Figure S3a–c (from the Supplementary Materials), where the XPS measurement of C 1 s spectra on the material surfaces can be decomposed into four individual Gaussian curves, with the identified binding energy peaks of 284.6 eV, 286.1 eV, 289.1 eV and 291.6 eV. Correspondingly, they belong to the functional groups of C-C/C-H, C-O, COO<sup>−</sup> and  $\pi = \pi^*$  shake-up, respectively [44,45]. Because the C-C/C-H bonds are characterized by the non-polar properties, their emergence is responsible for the hydrophobic behavior of the material surface. In other words, the accumulative adsorption of non-polar C-C/C-H bonds would like to gradually deteriorate the superhydrophilicity on the material surface. Now a more general question is raised concerning how to effectively prevent the adsorption of such a non-polar hydrophobic group on the material surface, so that the superhydrophilic phenomenon will persist in a long time.

Usually, after the femtosecond laser interaction with the materials, some uncoordinated metal cations can be created on the surface to result in the strong electron acceptability. In our case, there should be a massive Al<sup>3+</sup> cations generated on the sapphire surface through the hot nonequilibrium plasma formation, which is produced by the femtosecond laser processing. As a result, the carboxylate radical anions COO<sup>−</sup> can be naturally absorbed with the surface cations Al<sup>3+</sup>, and then develop into a stable chemisorbed carboxylate layer [46], as shown in Figure 2a. Because the saturated hydrocarbon chains extending outward from the carboxylate layer turn to be non-polar, both the wettability and the subsequent adsorption behaviors of the surface will be affected. When the non-polar saturated hydrocarbon chains continue to adsorb the non-polar groups in air with the lapse of time, a dense physically adsorbed hydrophobic layer can be formed on the sample surface. Under such circumstances, the superhydrophilicity is apt to converse into the hydrophobic.

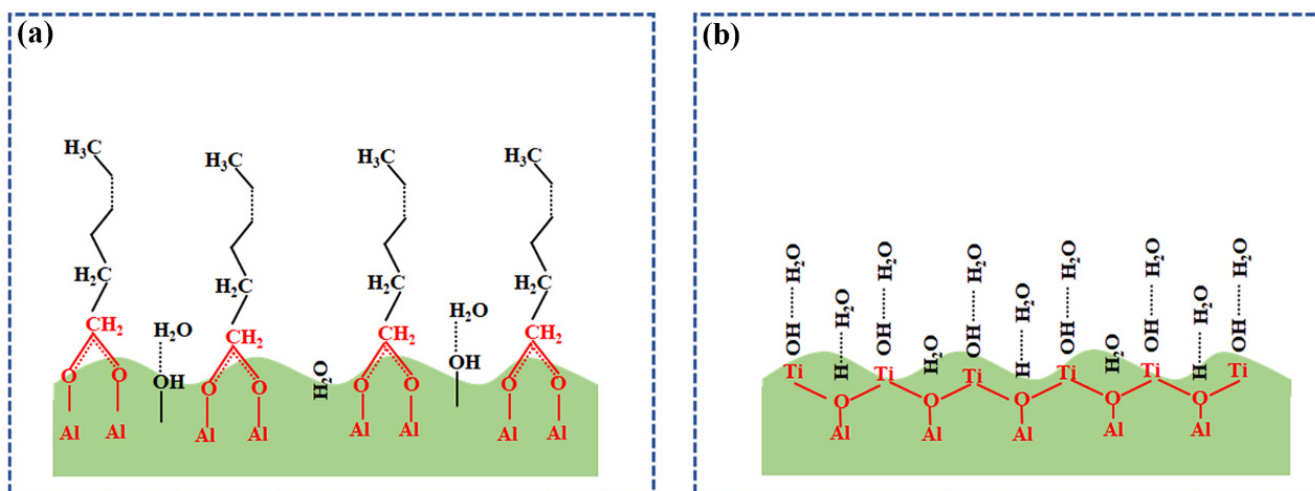


**Figure 2.** Schematic diagram for depiction of the superhydrophilic evolution on the sapphire surface under different conditions. (a) Chemisorption of non-polar saturated hydrocarbon chains on the laser-treated surface to make the superhydrophilic persistence shorter and conversion into the hydrophobicity; (b) Coordination of metal ions on the laser-structured sapphire surface by TiO<sub>2</sub> varnish to allow the adsorption of hydrophilic group for extending the superhydrophilic durability.

### 3.2. Superhydrophilic Persistence Improved by the Varnish of TiO<sub>2</sub>

Based on the above analyses, we suppose that if the Al<sup>3+</sup> ions on the sapphire surface produced by the laser processing are coordinated or covered by other substances to block their chemical links with COO<sup>−</sup> group and finally inhibit the subsequent adsorption of C-C/C-H, the observation of the extremely superhydrophilic can be possibly well maintained. Towards this goal, we chose the TiO<sub>2</sub> material with the phototropic superhydrophilic property to hinder the adsorption of Al<sup>3+</sup> and COO<sup>−</sup>, the preparation of which was described in Section 2.3. The annealing treatment not only transferred the TiO<sub>2</sub> precursor into anatase crystals but also presented Al<sup>3+</sup> doping into them. In other words, the naked Al<sup>3+</sup> ions on the sapphire surfaces can be coordinated via such a process, which consequently hinders the chemisorption of COO<sup>−</sup> for the transition of the superhydrophilic into the superhydrophobic. For convenience, here we would like to call the laser-processed surface with the TiO<sub>2</sub> varnish as “Laser-TiO<sub>2</sub>” surface.

As a result, the superhydrophilicity for all the samples becomes evidently prolonged after the varnish of TiO<sub>2</sub>, and their durable performances depend on the morphology of the surface structures induced by different laser-scanning speeds. Figure 3 illustrates the measured evolution of the contact angle for the different samples with the storing days without the additional UV illumination. In comparison to the results without the TiO<sub>2</sub> varnish (see Figure S2 from the Supplementary Materials), we find that at  $V = 0.5$  mm/s the extreme superhydrophilicity of the Laser-TiO<sub>2</sub> surfaces is prolonged to about half a month, while at  $V = 0.3$  mm/s the persistent time of the extreme superhydrophilic can be extended to about 60 days. Remarkably, in the case of  $V = 0.1$  mm/s, the superhydrophilic performance with  $CA = 0^\circ$  can be well maintained as long as 180 days (see video S2 from the Supplementary Materials), and the superhydrophilic behavior completely disappears after 200 days (see Figure S4 from the Supplementary Materials). Furthermore, from the change of the measured curves at the larger scanning speeds, we also find that the transformation from the superhydrophilic to the hydrophobic effects is slowed down on the surface of the Laser-TiO<sub>2</sub> samples.



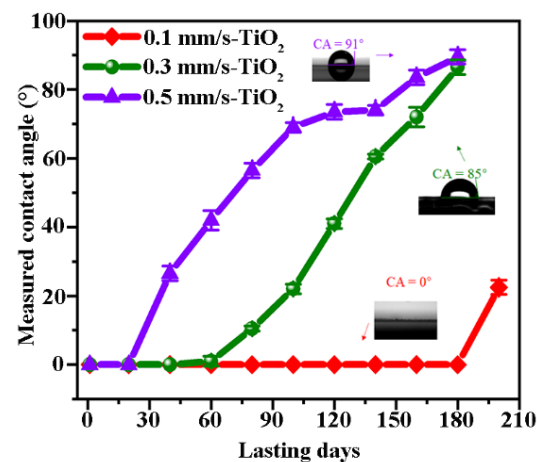


**Figure 3.** Measured evolution of the superhydrophilic persistence on the surface of Laser-TiO<sub>2</sub> samples with time elapsing.

### 3.3. Mechanisms of the Long-Term Persisting Superhydrophilic Effect

To comprehensively understand the underlying mechanisms of this strategy, we performed XRD, XPS and Raman measurements of the Laser-TiO<sub>2</sub> surfaces, as shown in Figure 4. From the XPS results of C 1 s in Figure 4a–c, we easily find that the adsorption of hydrophilic carboxyl -COOH (288.5 eV) happens on all the samples [47], which makes a sharp contrast to the observed absorption of the COO<sup>-</sup> group without the varnish of TiO<sub>2</sub> (see Figure S3a–c from the Supplementary Materials). Accordingly, the terminal parts of the long chain of amphiphilic hydrocarbon derivatives are no longer allowed to physically adsorb the non-polar saturated alkanes, leading to the unlikely transformation of the superhydrophilic into the hydrophobic on the surface. This indicates that the laser-induced Al<sup>3+</sup> ions are not present separately anymore and they are probably coordinated by doping with TiO<sub>2</sub> material, as shown in Figure 2b.

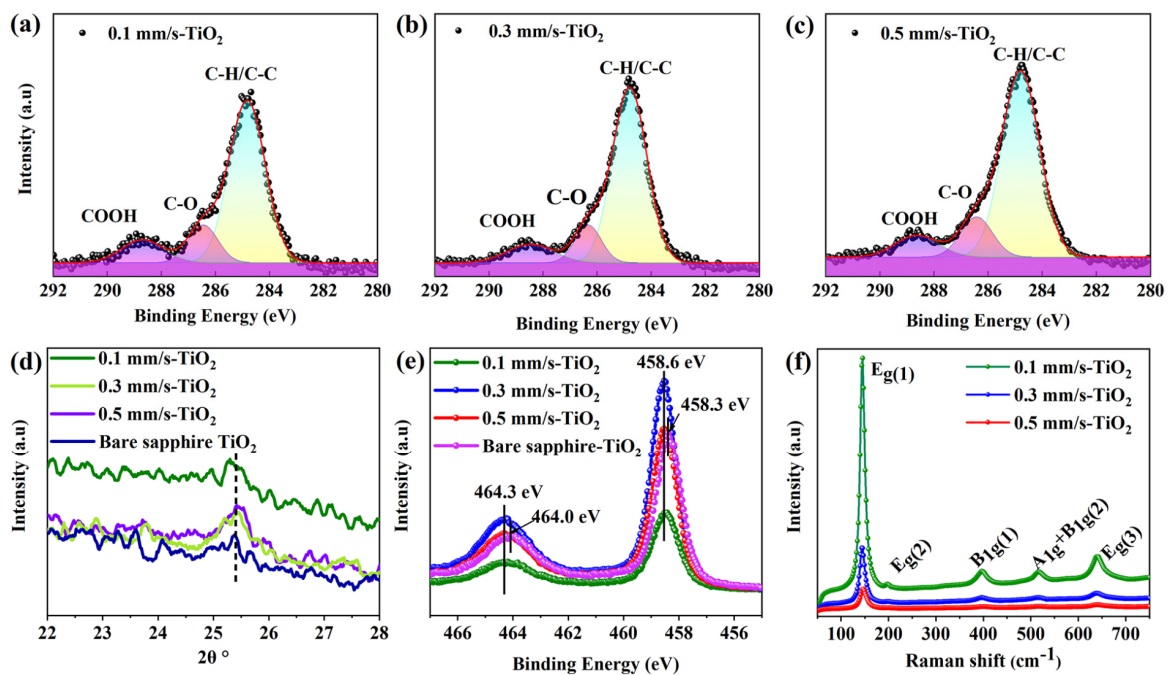


**Figure 4.** Characterization of the chemical change on Laser-TiO<sub>2</sub> surfaces. (a–c) Measured XPS results of C 1 s spectra for the Laser-TiO<sub>2</sub> surfaces with different scanning speeds; (d–f) Measured XRD, XPS (Ti 2 p), Raman spectra for the Laser-TiO<sub>2</sub> surfaces with different scanning speeds.

In addition, from the results of the XRD measurement in Figure 4d, we can see the characteristic peak at  $2\theta = 25.4^\circ$  (corresponding to a  $\langle 101 \rangle$  crystal plane of the anatase), which indicates the existence of the anatase  $\text{TiO}_2$  after the annealing process. Compared with both situations of  $V = 0.3$  mm/s and  $0.5$  mm/s, a blue shift of the peak position happening for  $V = 0.1$  mm/s suggests more  $\text{Al}^{3+}$  ions doping into the titanium dioxide [48]. Furthermore, the measured XPS results of Ti 2p in Figure 4e show that, for the bare sapphire surface, the peaks at 458.3 eV and 464 eV are attributed to the Ti-O-Ti bond in the anatase, whereas for the Laser- $\text{TiO}_2$  samples, the two peak positions of Ti 2p shift toward the higher binding energies of 458.6 eV and 464.3 eV, respectively, which also imply the doping of  $\text{Al}^{3+}$  ions into the  $\text{TiO}_2$  material [49]. In particular, the emergence of the binding energy at 458.6 eV can be attributed to the formation of the  $\text{Al}_2\text{TiO}_5$  material [50], which provides more strong evidence for  $\text{Al}^{3+}$  ions doping into the  $\text{TiO}_2$  substance.

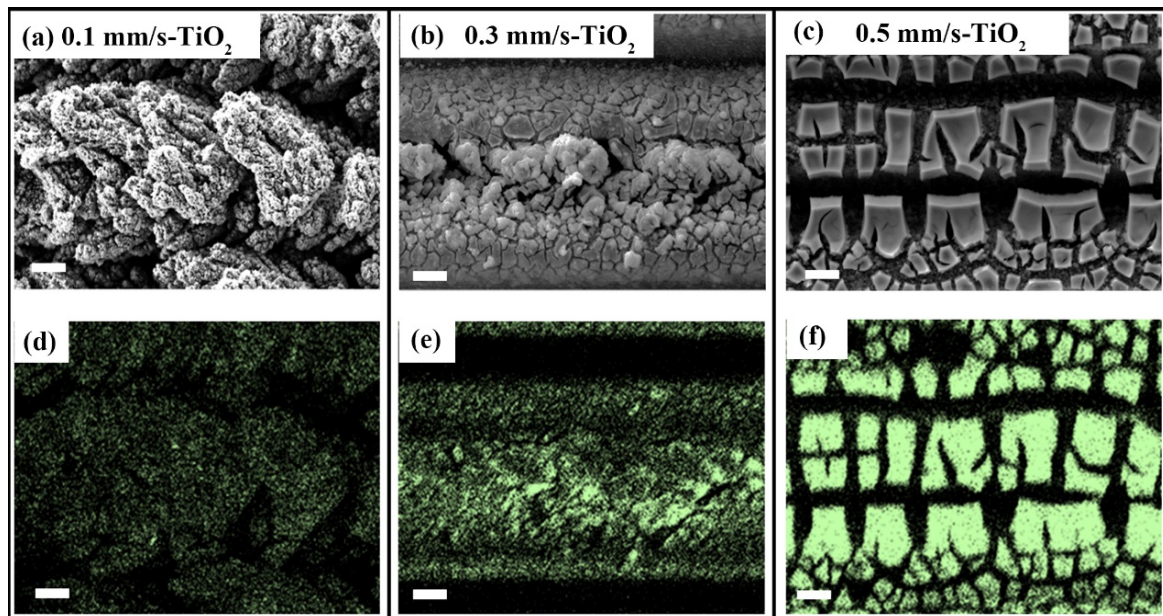
In terms of  $\text{TiO}_2$  doped by metal ions, many previous studies have confirmed that this would help to form the impurity energy levels within the bandgap and act as capture centers for the photogenerated electrons (or holes), so that the recombination of the photo-generated electron-hole pairs can be reduced to prolong the hydrophilicity of the material surface [51–53]. Remarkably, the decreasing in the bandgap can extend the photo response of  $\text{TiO}_2$  to the visible light region [54], thus improving the superhydrophilic effect without the UV light illumination.

Figure 4f shows the Raman spectra of the samples. The characteristic peaks at  $144\text{ cm}^{-1}$ ,  $196\text{ cm}^{-1}$ ,  $638\text{ cm}^{-1}$  and  $394\text{ cm}^{-1}$  belong to the active  $E_{g(1)}$ ,  $E_{g(2)}$ ,  $E_{g(3)}$  and  $B_{1g}$  vibrational modes of the anatase material, respectively, and the  $516\text{ cm}^{-1}$  peak represents a dual vibrational  $A_{1g}$  and  $B_{1g}$  modes [55]. More interestingly, the available Raman peaks for Laser- $\text{TiO}_2$  samples appear to be different in both the sharpness and the intensity with variable scanning speeds. For example, the peaks for  $V = 0.1$  mm/s are much sharper and intense than those of the  $V = 0.3$  mm/s and  $0.5$  mm/s cases. These results indicate that, for the surface with the small scanning speed, the growth of  $\text{TiO}_2$  substance tends to have the high crystallinity after the high-temperature annealing, which consequently slows down the electron-hole recombination rate to prolong the hydrophilicity.

Apart from affecting the crystallinity of  $\text{TiO}_2$ , the doping of metal ions also tends to inhibit the grain growth of  $\text{TiO}_2$  and prevent its transformation into rutile during the annealing process. Figure 5a–c show the surface morphology of the Laser- $\text{TiO}_2$  sample. The surface with  $V = 0.1$  mm/s is covered by many micron-scale clusters consisting of many nanoparticles to show a hierarchical structure, i.e., it has a larger roughness in surface morphology. This composite structure would like to exhibit the stronger capillary force. Through comparing their element distribution situations shown in Figure 5d–f, we find that, at the small laser-scanning speed of  $0.1$  mm/s, the ultrafine grains of  $\text{TiO}_2$  are almost uniformly dispersed among the multi-layer microstructures, almost without sacrifice of the surface roughness. However, for the larger scanning speeds, especially for the case of  $V = 0.5$  mm/s, the evident aggregation of the  $\text{TiO}_2$  substance within the laser-ablated trenches would like to decrease the surface roughness or make the surface appearance smoother (compared with Figure S1 from the Supplementary Materials). Obviously, the achieved  $\text{TiO}_2$  crystals on the hierarchical structures can inevitably allow more absorption of photons.

According to the theoretical calculations on the energy band structure change of the anatase  $\text{TiO}_2$  after the metal ions doping [56], we can deduce that the bandgap of our  $\text{Al}^{3+}$  doped  $\text{TiO}_2$  film presents a decreasing trend, as shown in Figure 6a. In fact, such a modulation of the energy band was further confirmed by the comparative measurements of the UV-Vis absorption spectroscopy for the different samples, and the results are shown in Figure 6b. It is seen that for the surface of the  $\text{TiO}_2$ -varnished bare sapphire material, the strong optical absorption occurs only in the UV range and presents a sharp cut-off wavelength at around  $\lambda = 387$  nm, in accordance with the previous report [57]. However, for the Laser- $\text{TiO}_2$  surfaces, the enhanced optical absorption takes place within the whole UV-Vis range. Specifically, for the case of  $V = 0.1$  mm/s the optical absorption within the

visible range can unprecedentedly improve to near 40%, which certainly helps to make the superhydrophilic of  $\text{TiO}_2$  more sensitive to both the wavelength and the intensity of light. At the same time, because of the generation of the  $\text{Al}_2\text{TiO}_5$  material with a narrower bandgap on the surface, which corresponds to a longer absorption cut-off wavelength stretching to a visible range [58], the optical absorption spectra of the Laser- $\text{TiO}_2$  surface are reasonably expanded.



**Figure 5.** Characterization of the surface morphology and the elemental distribution for the Laser- $\text{TiO}_2$  samples. (a–c) Variable morphology profiles at three different scanning speeds after femtosecond laser processing; (d–f) Observation of the elemental distribution patterns on the surfaces of three different scanning speeds. The green color for Ti element. Scale bars are 10  $\mu\text{m}$ .

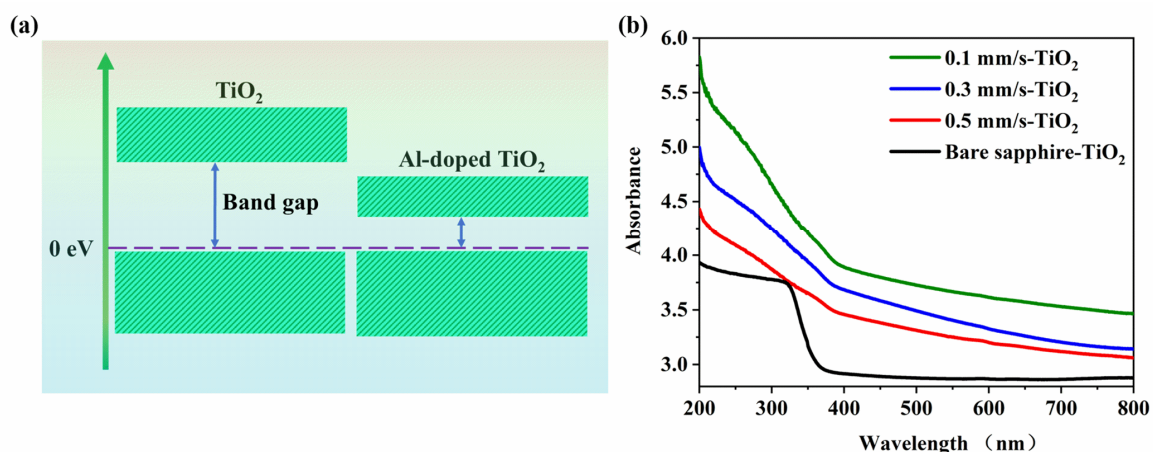


**Figure 6.** (a) Modified energy band structure of  $\text{TiO}_2$  by doping of  $\text{Al}^{3+}$  ions; (b) Measured absorption spectra for the surface of Laser- $\text{TiO}_2$  samples.

### 3.4. Potential Applications of the Superhydrophilic Laser- $\text{TiO}_2$ Surface

To further explore the potential applications of our samples, we carried out the anti-fogging tests with the continuous spraying of steam. The corresponding process and results are shown in Figure 7. At the spraying time of  $t = 6$  s, the periphery surface of the laser processing begins to be fogged, while the centrally positioned Laser- $\text{TiO}_2$  region is kept from the vapor condensation. As a matter of fact, this experimental observation



can be more pronounced with the continuous increase in the spraying time up to  $t = 23$  s, whereas the whole Laser-TiO<sub>2</sub> surface can remain clear and dry without any water traces, in sharp contrast to the evident accumulation of the liquified water droplets on the periphery areas. Such phenomena suggest that the superhydrophilic Laser-TiO<sub>2</sub> surface can quickly evaporate the water by its spreading into the large-area thin water film, leading to the so-called anti-fogging effect.

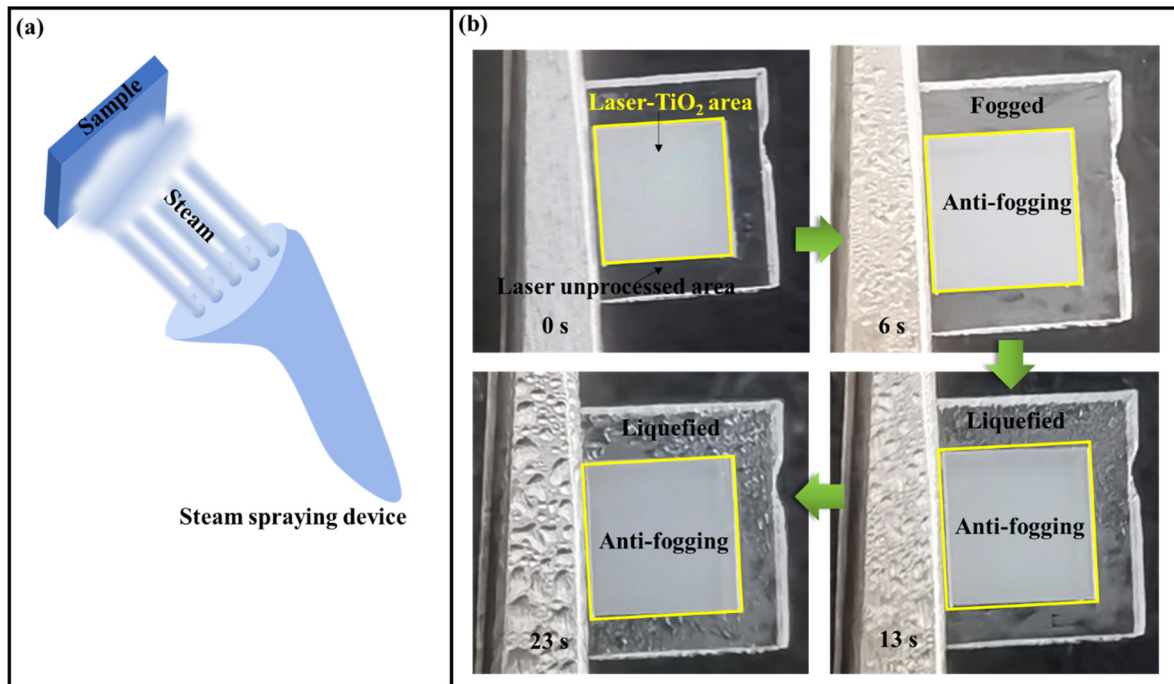


**Figure 7.** (a) A schematic illustration of the anti-fogging experiment; (b) Observation of anti-fogging behavior for the Laser-TiO<sub>2</sub> surface through the steam spraying processes.

#### 4. Conclusions

In summary, we comprehensively investigated how to make the widely used sapphire surface become the long-term sustainable superhydrophilic, especially with the contact angle of  $CA = 0^\circ$ , by proposing a method of femtosecond laser processing associated with the subsequent varnish of TiO<sub>2</sub>. Our main results include two parts. (i) We explain why the superhydrophilic properties of the sapphire surface cannot usually persist in a long time only by the femtosecond laser processing method. This is because a large number of uncoordinated Al<sup>3+</sup> ions can be generated through the femtosecond laser ablation, and subsequently their chemisorption with the COO<sup>-</sup> group tend to develop a carboxylate layer, whose terminal is apt to adsorb more hydrophobic groups over time. Therefore, the initially observed superhydrophilic effect eventually transfers into the hydrophobic surface. (ii) In order to effectively extend the superhydrophilic persistence (especially with  $CA = 0^\circ$ ) of the sapphire surface after the laser processing, we employed spin-coating of TiO<sub>2</sub> on the laser-structured surface and the subsequent heating treatment. This approach eventually resulted in the remarkable long-term superhydrophilic persistence of as long as 180 days. After comprehensive investigations, we believe that the coordination of Al<sup>3+</sup> ions with TiO<sub>2</sub> via doping tends to prevent the chemisorption of COO<sup>-</sup> groups and the further adsorption of other hydrophobic groups. Meanwhile, the optical response of the varnished sample surface can be extended into the whole UV-Vis wavelength range. Moreover, the doping of metal ions also inhibited the growth of the anatase grains, which leaves the high degree of the surface roughness to inevitably increase the absorption of photons. As a result, the superhydrophilic property of Laser-TiO<sub>2</sub> sample was achieved to persist for an unprecedentedly long time.

Finally, the potential applications of the samples were explored through the continuous spraying of steam on them. It was found that with the variation of spray time, the Laser-TiO<sub>2</sub> surface showed an excellent anti-fogging performance due to its excellent superhydrophilic property. We hope all these investigations will benefit the design and fabrication of the superhydrophilic surfaces for future usages.

**Supplementary Materials:** The following supporting information can be downloaded at: <https://www.mdpi.com/article/10.3390/nano12193403/s1>, Figure S1: Observation of the surface morphologies after femtosecond laser processing with different scanning speeds (a–c). Scale bars are 30 μm.; Figure S2: Measured superhydrophilic permanence over the time for three different samples without TiO<sub>2</sub> varnish. Superhydrophilic (CA = 0°) property of V=0.1, 0.3, 0.5 mm/s can be maintained for 45 days, 17 days and a few days, respectively; Figure S3: Measured XPS results of C 1s spectra for the laser treated samples with different scanning speeds (a–c); Figure S4: Measured XPS results of the sample surfaces before and after losing the superhydrophilicity. Clearly, there is a significant increase in the hydrophobic group C-C/C-H; moreover, the atomic percentage of the carbon element on the surface is increased by 9.42%. This indicates that some uncoordinated Al<sup>3+</sup> ions are still present on the structured surface; Video S1: A superhydrophilic surface with CA = 0° on the sapphire material by the laser ablation processing. Video S2: The superhydrophilic performance with CA = 0° can be well maintained as long as 180 days.

**Author Contributions:** Conceptualization, D.Y., Z.Y. and J.Y.; formal analysis, all authors; writing—original draft preparation, D.Y., Z.Y., T.Z. and J.Y.; data curation, D.Y. and Y.L.; Resources, D.Y. and W.K., writing—review and editing, D.Y., Z.Y., T.Z. and J.Y.; visualization, D.Y. and Y.L.; supervision, J.Y.; project administration, Z.Y. and J.Y.; funding acquisition, Z.Y. and J.Y. All authors have read and agreed to the published version of the manuscript.

**Funding:** This research was funded by [the Strategic Priority Research Program of Chinese Academy of Sciences], grant number [XDA22010302] and by [National Natural Science Foundation of China], grant number [11674178] and by [K. C. Wong Education Foundation], grant number [GJTD–2018–08] and by [Jilin Provincial Science & Technology Development Project], grant number [20200201086JC].

**Data Availability Statement:** Not applicable.

**Conflicts of Interest:** The authors declare no conflict of interest.

## References

1. Gu, J.; Ji, L.; Xiao, P.; Zhang, C.; Li, J.; Yan, L.; Chen, T. Recent Progress in Superhydrophilic Carbon-Based Composite Membranes for Oil/Water Emulsion Separation. *ACS Appl. Mater. Interfaces* **2021**, *13*, 36679–36696. [[CrossRef](#)]
2. Zhang, G.; Liu, Y.; Chen, C.; Huang, C.; Long, L.; Zhang, S.; Yang, G.; Shen, F.; Zhang, X.; Zhang, Y. Green, robust self-cleaning superhydrophilic coating and on-demand oil–water separation. *Appl. Surf. Sci.* **2022**, *595*, 153472. [[CrossRef](#)]
3. Kim, P.; Wong, T.-S.; Alvarenga, J.; Kreder, M.J.; Adorno-Martinez, W.E.; Aizenberg, J. Liquid-Infused Nanostructured Surfaces with Extreme Anti-Ice and Anti-Frost Performance. *ACS Nano* **2012**, *6*, 6569–6577. [[CrossRef](#)]
4. Adera, S.; Raj, R.; Enright, R.; Wang, E.N. Non-wetting droplets on hot superhydrophilic surfaces. *Nat. Commun.* **2013**, *4*, 2518. [[CrossRef](#)]
5. Paradisanos, I.; Fotakis, C.; Anastasiadis, S.; Stratakis, E. Gradient induced liquid motion on laser structured black Si surfaces. *Appl. Phys. Lett.* **2015**, *107*, 111603. [[CrossRef](#)]
6. Tan, E.-L.; Potroz, M.G.; Ferracci, G.; Wang, L.; Jackman, J.A.; Cho, N.-J. Hydrophobic to superhydrophilic tuning of multifunctional sporopollenin for microcapsule and bio-composite applications. *Appl. Mater. Today* **2019**, *18*, 100525. [[CrossRef](#)]
7. Raittinen, P.; Elomaa, P.; Saavalainen, P.; Jokinen, V. Single Cell Trapping by Superhydrophobic/Superhydrophilic Microarrays. *Adv. Mater. Interfaces* **2021**, *8*, 2100147. [[CrossRef](#)]
8. Liu, Y.; Wang, X.; Zhang, Y.; Zhang, C.; Luo, L.; Lai, W.; Li, Y.; Liu, X. In-situ generation of hydrated nanoparticles on commercial stainless steel mesh for durable superhydrophilicity and self-cleaning. *Mater. Des.* **2018**, *157*, 284–293. [[CrossRef](#)]
9. Chai, O.J.H.; Wu, Z.; Xie, J. All Hydroxyl-Thiol-Protected Gold Nanoclusters with Near-Neutral Surface Charge. *J. Phys. Chem. Lett.* **2021**, *12*, 9882–9887. [[CrossRef](#)]
10. Bain, C.D.; Troughton, E.B.; Tao, Y.T.; Evall, J.; Whitesides, G.M.; Nuzzo, R.G. Formation of monolayer films by the spontaneous assembly of organic thiols from solution onto gold. *J. Am. Chem. Soc.* **1989**, *111*, 321–335. [[CrossRef](#)]
11. Laibinis, P.E.; Bain, C.D.; Whitesides, G.M. Attenuation of photoelectrons in monolayers of n-alkanethiols adsorbed on copper, silver, and gold. *J. Phys. Chem.* **1991**, *95*, 7017–7021. [[CrossRef](#)]
12. Laibinis, P.E.; Whitesides, G.M. ω-Terminated alkanethiolate monolayers on surfaces of copper, silver, and gold have similar wettabilities. *J. Am. Chem. Soc.* **1992**, *114*, 1990–1995. [[CrossRef](#)]

13. Laibinis, P.E.; Whitesides, G.M.; Allara, D.L.; Tao, Y.T.; Parikh, A.N.; Nuzzo, R.G. Comparison of the structures and wetting properties of self-assembled monolayers of n-alkanethiols on the coinage metal surfaces, copper, silver, and gold. *J. Am. Chem. Soc.* **1991**, *113*, 7152–7167. [[CrossRef](#)]
14. Choong, L.F.; Cheong, K.Y.; Ramakrishnan, S.; Roslan, A.F. The adhesion of epoxy treated by microwave oxygen plasma. *Appl. Surf. Sci.* **2021**, *563*, 150224. [[CrossRef](#)]
15. Yoo, S.; Seok, D.; Jung, Y.; Lee, K. Hydrophilic Surface Treatment of Carbon Powder Using CO<sub>2</sub> Plasma Activated Gas. *Coatings* **2021**, *11*, 925. [[CrossRef](#)]
16. Chan, C.-M.; Ko, T.-M.; Hiraoka, H. Polymer surface modification by plasmas and photons. *Surf. Sci. Rep.* **1996**, *24*, 1–54. [[CrossRef](#)]
17. Liston, E.M.; Martinu, L.; Wertheimer, M.R. Plasma surface modification of polymers for improved adhesion: A critical review. *J. Adhes. Sci. Technol.* **1993**, *7*, 1091–1127. [[CrossRef](#)]
18. Tuominen, M.; Lahti, J.; Lavonen, J.; Penttinen, T.; Räsänen, J.P.; Kuusipalo, J. The Influence of Flame, Corona and Atmospheric Plasma Treatments on Surface Properties and Digital Print Quality of Extrusion Coated Paper. *J. Adhes. Sci. Technol.* **2010**, *24*, 471–492. [[CrossRef](#)]
19. Yong, J.; Chen, F.; Yang, Q.; Jiang, Z.; Hou, X. A Review of Femtosecond-Laser-Induced Underwater Superoleophobic Surfaces. *Adv. Mater. Interfaces* **2018**, *5*, 1701370. [[CrossRef](#)]
20. Hermens, U.; Kirner, S.; Emonts, C.; Comanns, P.; Skoulas, E.; Mimidis, A.; Mescheder, H.; Winands, K.; Krüger, J.; Stratakis, E.; et al. Mimicking lizard-like surface structures upon ultrashort laser pulse irradiation of inorganic materials. *Appl. Surf. Sci.* **2017**, *418*, 499–507. [[CrossRef](#)]
21. Yan, J.; Deng, S.; Zhu, D.; Bai, H.; Zhu, H. Self-powered SnSe photodetectors fabricated by ultrafast laser. *Nano Energy* **2022**, *97*, 107188. [[CrossRef](#)]
22. Singh, S.C.; Guo, C. Femtosecond laser-produced optical absorbers for solar-thermal energy harvesting. *EcoMat* **2021**, *4*, e12161. [[CrossRef](#)]
23. Ionin, A.A.; Kudryashov, S.I.; Makarov, S.V.; Saltuganov, P.N.; Seleznev, L.V.; Sinitsyn, D.V.; Golosov, E.V.; Goryainov, A.A.; Kolobov, Y.R.; Kornieieva, K.A.; et al. Femtosecond laser modification of titanium surfaces: Direct imprinting of hydroxylapatite nanopowder and wettability tuning via surface microstructuring. *Laser Phys. Lett.* **2013**, *10*, 45605. [[CrossRef](#)]
24. Cao, Q.; Wang, Z.; He, W.; Guan, Y. Fabrication of super hydrophilic surface on alumina ceramic by ultrafast laser microprocessing. *Appl. Surf. Sci.* **2021**, *557*, 149842. [[CrossRef](#)]
25. Singh, S.C.; ElKabbash, M.; Li, Z.; Li, X.; Regmi, B.; Madsen, M.; Jalil, S.A.; Zhan, Z.; Zhang, J.; Guo, C. Solar-trackable super-wicking black metal panel for photothermal water sanitation. *Nat. Sustain.* **2020**, *3*, 938–946. [[CrossRef](#)]
26. Baron, C.F.; Mimidis, A.; Puerto, D.; Skoulas, E.; Stratakis, E.; Solis, J.; Siegel, J. Biomimetic surface structures in steel fabricated with femtosecond laser pulses: Influence of laser rescanning on morphology and wettability. *Beilstein J. Nanotechnol.* **2018**, *9*, 2802–2812. [[CrossRef](#)] [[PubMed](#)]
27. Samanta, A.; Wang, Q.; Shaw, S.K.; Ding, H. Roles of chemistry modification for laser textured metal alloys to achieve extreme surface wetting behaviors. *Mater. Des.* **2020**, *192*, 108744. [[CrossRef](#)]
28. Chang, F.-M.; Cheng, S.-L.; Hong, S.-J.; Sheng, Y.-J.; Tsao, H.-K. Superhydrophilicity to superhydrophobicity transition of CuO nanowire films. *Appl. Phys. Lett.* **2010**, *96*, 114101. [[CrossRef](#)]
29. Bizi-Bandoki, P.; Valette, S.; Audouard, E.; Benayoun, S. Time dependency of the hydrophilicity and hydrophobicity of metallic alloys subjected to femtosecond laser irradiations. *Appl. Surf. Sci.* **2013**, *273*, 399–407. [[CrossRef](#)]
30. Lanara, C.; Mimidis, A.; Stratakis, E. Femtosecond Laser Fabrication of Stable Hydrophilic and Anti-Corrosive Steel Surfaces. *Materials* **2019**, *12*, 3428. [[CrossRef](#)]
31. Rajab, F.; Liu, Z.; Li, L. Production of stable superhydrophilic surfaces on 316L steel by simultaneous laser texturing and SiO<sub>2</sub> deposition. *Appl. Surf. Sci.* **2018**, *427*, 1135–1145. [[CrossRef](#)]
32. Rajan, R.A.; Ngo, C.-V.; Yang, J.; Liu, Y.; Rao, K.; Guo, C. Femtosecond and picosecond laser fabrication for long-term superhydrophilic metal surfaces. *Opt. Laser Technol.* **2021**, *143*, 107241. [[CrossRef](#)]
33. Wang, R.; Hashimoto, K.; Fujishima, A.; Chikuni, M.; Kojima, E.; Kitamura, A.; Shimohigoshi, M.; Watanabe, T. Light-induced amphiphilic surfaces. *Nature* **1997**, *388*, 431–432. [[CrossRef](#)]
34. Sun, J.J.; Sun, J.; Wang, X.K. Anatase TiO<sub>2</sub> with Co-exposed (001) and (101) Surface-Based Photocatalytic Materials for Energy Conversion and Environmental Purification. *Chem. Asian J.* **2020**, *15*, 4168–4183. [[CrossRef](#)] [[PubMed](#)]
35. Li, Z.; Wang, S.; Wu, J.; Zhou, W. Recent progress in defective TiO<sub>2</sub> photocatalysts for energy and environmental applications. *Renew. Sustain. Energy Rev.* **2021**, *156*, 111980. [[CrossRef](#)]
36. Duan, Z.; Zhu, Y.; Ren, P.; Jia, J.; Yang, S.; Zhao, G.; Xie, Y.; Zhang, J. Non-UV activated superhydrophilicity of patterned Fe-doped TiO<sub>2</sub> film for anti-fogging and photocatalysis. *Appl. Surf. Sci.* **2018**, *452*, 165–173. [[CrossRef](#)]
37. Miyauchi, M.; Nakajima, A.; Hashimoto, K.; Watanabe, T. A highly hydrophilic thin film under 1 μW/cm<sup>2</sup> UV illumination. *Adv. Mater.* **2000**, *12*, 1923–1927. [[CrossRef](#)]
38. Choi, W.; Termin, A.; Hoffmann, M.R. The Role of Metal Ion Dopants in Quantum-Sized TiO<sub>2</sub>: Correlation between Photoreactivity and Charge Carrier Recombination Dynamics. *J. Phys. Chem.* **1994**, *98*, 13669–13679. [[CrossRef](#)]
39. Keerthana, S.; Yuvakkumar, R.; Ravi, G.; Hong, S.; Al-Sehemi, A.G.; Velauthapillai, D. Fabrication of Ce doped TiO<sub>2</sub> for efficient organic pollutants removal from wastewater. *Chemosphere* **2022**, *293*, 133540. [[CrossRef](#)]

40. Low, J.; Cheng, B.; Yu, J. Surface modification and enhanced photocatalytic CO<sub>2</sub> reduction performance of TiO<sub>2</sub>: A review. *Appl. Surf. Sci.* **2017**, *392*, 658–686. [[CrossRef](#)]
41. Zhang, K.; Yin, L.; Liu, G.; Cheng, H.-M. Accurate structural descriptor enabled screening for nitrogen and oxygen vacancy codoped TiO<sub>2</sub> with a large bandgap narrowing. *J. Mater. Sci. Technol.* **2022**, *122*, 84–90. [[CrossRef](#)]
42. Chen, F.; Zhang, D.; Yang, Q.; Yong, J.; Du, G.; Si, J.; Yun, F.; Hou, X. Bioinspired Wetting Surface via Laser Microfabrication. *ACS Appl. Mater. Interfaces* **2013**, *5*, 6777–6792. [[CrossRef](#)] [[PubMed](#)]
43. Kietzig, A.-M.; Hatzikiriakos, S.G.; Englezos, P. Patterned Superhydrophobic Metallic Surfaces. *Langmuir* **2009**, *25*, 4821–4827. [[CrossRef](#)]
44. Long, J.; Zhong, M.; Fan, P.; Gong, D.; Zhang, H. Wettability conversion of ultrafast laser structured copper surface. *J. Laser Appl.* **2015**, *27*, S29107. [[CrossRef](#)]
45. Zong, M.; Huang, Y.; Wu, H.; Zhao, Y.; Liu, P.; Wang, L. Facile preparation of RGO/Cu<sub>2</sub>O/Cu composite and its excellent microwave absorption properties. *Mater. Lett.* **2013**, *109*, 112–115. [[CrossRef](#)]
46. Li, J.; Li, C.; Yang, G.; Li, C. Wettability transition on micro-nano hierarchical structured Ni<sub>20</sub>Cr coating surface by selective spontaneous adsorption during vacuum evacuation. *Mater. Chem. Phys.* **2018**, *219*, 292–302. [[CrossRef](#)]
47. Liu, P.; Cao, L.; Zhao, W.; Xia, Y.; Huang, W.; Li, Z. Insights into the superhydrophobicity of metallic surfaces prepared by electrodeposition involving spontaneous adsorption of airborne hydrocarbons. *Appl. Surf. Sci.* **2015**, *324*, 576–583. [[CrossRef](#)]
48. Lin, S.-S.; Wu, D.-K. The properties of Al-doped TiO<sub>2</sub> nanoceramic films deposited by simultaneous rf and dc magnetron sputtering. *Ceram. Int.* **2010**, *36*, 87–91. [[CrossRef](#)]
49. Neetu, M.; Maurya, I.C.; Gupta, A.K.; Srivastava, P.; Bahadur, L. Extensive enhancement in power conversion efficiency of dye-sensitized solar cell by using Al-doped TiO<sub>2</sub> photoanode. *J. Solid State Electrochem.* **2016**, *21*, 1229–1241. [[CrossRef](#)]
50. Armelao, L.; Martucci, A.; Innocenzi, P. Study of β-Al<sub>2</sub>TiO<sub>5</sub> Thin Films by XPS. *Surf. Sci. Spectra* **2001**, *8*, 8–13. [[CrossRef](#)]
51. Jing, T.; Zhang, P.; Kan, W.; Tian, J.; Deng, Q. Theory studies on electronic structure and optical properties of N-Al co-doped anatase TiO<sub>2</sub>. *Chin. J. Nonferrous Met.* **2015**, *25*, 1018–1024.
52. Liu, Z.; Wang, Y.; Peng, X.; Li, Y.; Liu, Z.; Liu, C.; Ya, J.; Huang, Y. Photoinduced superhydrophilicity of TiO<sub>2</sub> thin film with hierarchical Cu doping. *Sci. Technol. Adv. Mater.* **2012**, *13*, 025001. [[CrossRef](#)] [[PubMed](#)]
53. Lee, Y.C.; Hong, Y.P.; Lee, H.Y.; Kim, H.; Jung, Y.J.; Ko, K.H.; Jung, H.S.; Hong, K.S. Photocatalysis and hydrophilicity of doped TiO<sub>2</sub> thin films. *J. Colloid Interface Sci.* **2003**, *267*, 127–131. [[CrossRef](#)]
54. Yang, S.M.; Zhu, G.H.; Guo, S.P. Effects of Al on the Flat Band Potential of Nanostructured TiO<sub>2</sub> Electrodes. *Appl. Mech. Mater.* **2013**, *291–294*, 2731–2733. [[CrossRef](#)]
55. Frank, O.; Zukulova, M.; Laskova, B.; Kürti, J.; Koltai, J.; Kavan, L. Raman spectra of titanium dioxide (anatase, rutile) with identified oxygen isotopes (16, 17, 18). *Phys. Chem. Chem. Phys.* **2012**, *14*, 14567–14572. [[CrossRef](#)] [[PubMed](#)]
56. Farzaneh, A.; Javidani, M.; Esrafil, M.D.; Mermer, O. Optical and photocatalytic characteristics of Al and Cu doped TiO<sub>2</sub>: Experimental assessments and DFT calculations. *J. Phys. Chem. Solids* **2021**, *161*, 110404. [[CrossRef](#)]
57. Asahi, R.; Morikawa, T.; Ohwaki, T.; Aoki, K.; Taga, Y. Visible-Light Photocatalysis in Nitrogen-Doped Titanium Oxides. *Science* **2001**, *293*, 269–271. [[CrossRef](#)]
58. Kim, S.; Lee, M.; Hong, C.; Yoon, Y.; An, H.; Lee, D.; Jeong, W.; Yoo, D.; Kang, Y.; Youn, Y.; et al. A band-gap database for semiconducting inorganic materials calculated with hybrid functional. *Sci. Data* **2020**, *7*, 387. [[CrossRef](#)]